

# Iterative Carrier Frequency Offset and Channel Estimation for Underwater Acoustic OFDM Systems

Taehyuk Kang, *Student Member, IEEE*, and Ronald A. Iltis, *Senior Member, IEEE*

**Abstract**—This paper presents a practical low-density parity-check (LDPC) coded OFDM system designed for the underwater acoustic channel with its attendant sparse multipath channel and Doppler effects. The carrier frequency offset (CFO) and channel state information (CSI) are assumed unavailable to both to the transmitter and the receiver. Several different receiver structures are considered, all of which perform CFO/channel estimation, detection and decoding in an iterative manner. The convergence behavior of the iterative receivers and their asymptotic performance are evaluated using the extrinsic information transfer (EXIT) chart method. OFDM receiver performance is further evaluated through simulations and field tests in shallow water.

**Index Terms**—OFDM, low-density parity-check codes, underwater acoustic communications, iterative receiver, carrier frequency offset, Matching Pursuits, EXIT chart.

## I. INTRODUCTION

THE FUNDAMENTAL obstacles to robust underwater acoustic communications (UAC) are the long multipath delay and large Doppler effects [1], [2]. The main advantage of Orthogonal Frequency Division Multiplexing (OFDM) is that since each subcarrier only experiences flat fading, complex time-domain equalizers are not necessary [3]. Thus, OFDM is an attractive choice for such a channel as the cyclic prefix (CP) eliminates intersymbol interference (ISI) and high data rates using coherent transmission can be achieved. While OFDM provides simple channel equalization in the frequency domain, it is well known that its performance is sensitive to CFO due to local oscillator mismatches and Doppler shifts caused by motion. CFO destroys the orthogonality of the subcarriers, thus causing intercarrier interference (ICI) [4]. Due to the slow speed of sound in water ( $c = 1500$  m/s), even small platform motions can affect the performance of the system significantly [5], thus the time-varying CFO must be accurately tracked and compensated for. Therefore OFDM for the UAC requires agile and accurate tracking of the CFO and multipath channel.

We focus on robust receiver solutions where the CFO and channel are estimated on a symbol-by-symbol basis, in contrast to recursive nonlinear filtering algorithms which are subject to divergence [6], [7]. Current applications of OFDM to underwater communications appear in [5], [8]–[15]. Recently, zero-padded (ZP)-OFDM with the overlap-add method [8], [12]–[15] was introduced for UAC applications, where the

parameters are also estimated on a symbol-by-symbol basis, but iterative decoding/estimation is not considered. It is shown that ZP-OFDM may outperform CP-OFDM if appropriate receivers are used [16]. However, we focus on CP-OFDM here in order to a) avoid the SNR loss [17] incurred in ZP-OFDM with the overlap-add method and b) avoid the possible extra receiver complexity as in [16] to obtain the performance benefits of ZP-OFDM. There are many approaches in the literature to CFO tracking and CE for OFDM systems. In separable CFO/CE, channel independent CFO estimation is first performed [18]–[20], and the offset-corrected signal is used for CE [21], [22]. In [6], joint estimation is performed by the extended Kalman filter, in which the second-order statistics of the channel are assumed available. The CFOE/CE also can be performed iteratively [23]–[25]. Note however that [23]–[25] only consider uncoded systems. Iterative receivers for LDPC-coded OFDM over the UAC are studied here which are based on the Turbo principle. The Turbo principle was originally developed for decoding concatenated codes [26] and has since been applied to equalization [27], channel estimation [28]–[36], and synchronization [37].

The first contribution of the paper is the development of a channel estimator for UAC OFDM based on the Matching Pursuits (MP) algorithm [38]–[43]. We showed in [38] that MP is well suited to the UAC, since this channel is often very sparse [44]. Among existing CE techniques for OFDM, two-dimensional Wiener filtering [45] is optimal in the minimum mean-square error sense. However, such filtering has high computational complexity and requires accurate channel auto-correlation estimates which are difficult to obtain in the UAC. Conventional CE for OFDM is performed in the frequency domain [3]. However, time domain CE may be preferred in order to exploit the sparse nature of the channel [21]. An MP algorithm was also proposed for OFDM in [46], however, it assumes temporal channel correlation between symbols which might not be appropriate for the UAC.

The second contribution is that we design, analyze and compare different OFDM iterative receiver structures with decoding of LDPC codes [47], [48]. In order to design the iterative algorithm, two fundamental components are modeled for message-passing. For the first scheme (Fig. 1a), we partition the receiver into a) CFO/channel estimator and detector and b) LDPC decoder. For the second scheme (Fig. 1b), we partition the receiver into a) the “super decoder” (which consists of the variable node decoder in the LDPC decoder, CFO/channel estimators, and detector) and b) the check node decoder in the LDPC decoder, as in [49]. The main difference is that the

Manuscript received February 21, 2008; revised July 18, 2008. This work was supported in part by NSF grant No. ECCS-0742221.

The authors are with Department of Electrical and Computer Engineering, University of California, Santa Barbara, CA 93106-9560, USA (e-mail: {tkang, iltis}@ece.ucsb.edu).

Digital Object Identifier 10.1109/JSAC.2008.081205.



TABLE I: OFDM System specifications

FFT size ( $N_s$ )	512				
Number of Data subcarriers	336				
Number of pilots	48 (uniformly distributed)				
Cyclic prefix Ratio ( $R_{cp}$ )	1/8				
Carrier Frequency	24 KHz				
Bandwidth	4 KHz (22 - 26 KHz)				
Subcarrier BW	7.81 Hz				
Cyclic prefix duration	16 ms				
Symbol duration with CP	144 ms				
Data rate (uncoded/coded)	4666bps, 2333bps				
ADC/DAC Frequency	96 KHz (TI 6713C board)				
Modulation Order	QPSK				
CFO search resolution	512 points				
LDPC decoder	(672,336) half-rate 802.16e				
$d_{v,i}$	$a_{v,i}$	$b_{v,i}$	$d_{c,i}$	$a_{c,i}$	$b_{c,i}$
2	0.4583	0.2895	6	0.6666	0.6316
3	0.3333	0.3158	7	0.3333	0.3684
6	0.2083	0.3947	-	-	-

### A. Transmitter and Channel

Consider an OFDM system with  $N_s$  subcarriers and  $N_g$  Nyquist samples comprising the CP guard interval, so that  $N_g = R_{cp}N_s$  where  $R_{cp}$  is the ratio of the CP length to the total number of subcarriers. For an OFDM symbol duration  $T_s$ ,  $\Delta f = \frac{1}{T_s}$  is the subcarrier spacing. Pilot symbol assisted modulation (PSAM) [54] is applied. The bit sequence is LDPC encoded and interleaved bit-wise. Adjacent interleaved bit pairs are grouped and modulated via Gray coded QPSK. The pilot tones are then multiplexed with data symbols. The transmitted signal can be expressed as the sum of orthogonal pilots and data,  $s_k = p_k + d_k$  where  $p_k \times d_k = 0$  for  $0 \leq k \leq N_s - 1$ . Note  $p_k = d_k = 0$  in a guard band. We define a vector  $\mathbf{s} = [s_0, s_1, \dots, s_{N_s-1}]^T$  and vectors  $\mathbf{p}$  and  $\mathbf{d}$  are defined similarly, satisfying  $\mathbf{s} = \mathbf{p} + \mathbf{d}$ . The time-domain OFDM symbol  $\mathbf{t}$  is generated by the Inverse Fourier Transform (IFFT) ( $\mathbf{t} = \mathbf{W}^H \mathbf{s}$ ) where  $\mathbf{W} \in \mathbb{C}^{N_s \times N_s}$  is the FFT matrix, with  $W_{n,m} = \frac{1}{\sqrt{N_s}} e^{-i2\pi(n-1)(m-1)/N_s}$ . Then the CP is added such that  $\tilde{\mathbf{t}} = [t_{N_s-N_g}, \dots, t_{N_s-1}, t_0, \dots, t_{N_s-1}]^T$ .

The Doppler distortion can be quite severe in the UAC comprising both a bulk shift and spread. Following [8], [14], we model the Doppler effect as a pure CFO, i.e. a pure Doppler shift for algorithm development purposes. However, since the channel is estimated on a symbol-by-symbol basis, and assumed independent between symbols, our receivers can accommodate additional Doppler spreads that are a fraction of the symbol rate. Note that this CFO model for Doppler taken from [8], [14], although simplified, yielded a robust receiver design with excellent field test results at 12-20m depth and 0.5-2.5 km distance. This simplified model is applicable to shallow water transmission with range much greater than depth, where the multipath arrival angles are similar, and the Doppler shift effect is dominated by transmitter/receiver relative motion. The multipath channel and CFO are assumed to be static in one OFDM symbol but independent between symbols. Define the multi-path channel vector  $\mathbf{f} = [f_0, f_1, \dots, f_{N_f-1}]^T$ , where  $N_f$  is the maximum delay spread of the channel. We assume a sufficient CP length to avoid ISI ( $N_g \gg N_f$ ). In the presence of noise and CFO ( $\delta$ ), the  $n$ th received OFDM sample including the CP is,

$$y_n = \zeta_n e^{i2\pi\epsilon n/N_s} + n_n, \quad -N_g \leq n \leq N_s - 1, \quad (1)$$

where  $\zeta_n = \tilde{t}_n * f_n$ ,  $*$  is the convolution operator and  $\epsilon = \frac{\delta}{\Delta f}$  is the normalized CFO. In practice, the samples  $y_n$  are affected by a common accumulated phase due to CFO. However, since the channel is estimated independently on each symbol, the accumulated phase can be absorbed into each  $\zeta_n$  in (1).

### B. Receiver

It is convenient to express the received samples in vector form after CP removal. The channel matrix  $\mathbf{F} \in \mathbb{C}^{N_s \times N_s}$  is circulant with first column given by  $[f_0, f_1, \dots, f_{N_f-1}, 0, \dots, 0]^T$ . The frequency offset matrix  $\mathbf{E}(\epsilon) \in \mathbb{C}^{N_s \times N_s}$  is  $\mathbf{E}(\epsilon) = \text{diag}\{1, e^{i2\pi\epsilon/N_s}, \dots, e^{i2\pi(N_s-1)\epsilon/N_s}\}$ . Then the received sampled vector  $\mathbf{y} = [y_0, y_1, \dots, y_{N_s-1}]^T$  after removing the CP is,

$$\mathbf{y} = \mathbf{E}(\epsilon)\mathbf{F}\mathbf{W}^H \mathbf{s} + \mathbf{n}, \quad (2)$$

where  $\mathbf{n}$  is the additive noise. Although the noise  $\mathbf{n}$  in the UAC is typically non-Gaussian, it is approximated here as circular white Gaussian with covariance matrix  $\sigma_n^2 \mathbf{I}_{N_s}$  for algorithm development purposes following [5], [8].

Assume the estimate of CFO  $\hat{\epsilon}$  is available from CFOE, then CFO is removed in (2) by premultiplication, yielding  $\tilde{\mathbf{y}} = \mathbf{E}(\hat{\epsilon})^H \mathbf{y}$ . Then CE is performed by assuming there is no residual CFO distortion in  $\tilde{\mathbf{y}}$  ( $\hat{\epsilon} = \epsilon$ ). Note however that residual CFOE error is fully accounted for in the simulations. The fundamental receiver blocks in Fig. 1 are now summarized.

1) *Symbol Demapper (Detector)*: Assume the estimate of the channel  $\hat{\mathbf{f}} \in \mathbb{C}^{N_f}$  is available from CE, then  $\hat{\mathbf{f}}$  and  $\tilde{\mathbf{y}}$  are converted into the frequency domain via FFT,  $\hat{\mathbf{h}} = \sqrt{N_s} \mathbf{W} \hat{\mathbf{f}}$ ,  $\mathbf{z} = \mathbf{W} \tilde{\mathbf{y}}$ , where  $\tilde{\mathbf{f}} \in \mathbb{C}^{N_s}$  is the zero-padded version of  $\hat{\mathbf{f}}$ , followed by pilot removal. The extrinsic  $L$ -value of  $c_{j,i}$  (the  $i$ th coded bit of the  $j$ th data symbol  $d_j$ ) at the ‘‘symbol demapper’’ in Fig. 1 is given by (3), where  $L_{A,DET}(c_{j,i}) = \log \frac{p(c_{j,i}=1)}{p(c_{j,i}=0)}$  is the *a priori*  $L$ -value. The computation for  $L_{E,DET}(c_{j,2})$  similarly follows (3). The conditional density is given by

$$p(z_j | c_{j,1}, c_{j,2}, \hat{h}_j) = c \exp\left(-\frac{1}{\sigma_n^2} |z_j - \hat{h}_j d_j|^2\right). \quad (4)$$

Note that the  $e^{L_{A,DET}(c)}$  terms cancel out in (3) for Gray mapping QPSK modulation, thus the dashed line in Fig. 1 can be deleted for QPSK.

2) *LDPC Decoder*: We consider the half-rate (672,336) irregular LDPC code from the IEEE 802.16e standard [50]. The parameters of the code are in Table I, where  $b_{v,i}$  ( $b_{c,i}$ ) is the fraction of edges incident to variable (check) nodes of degree  $d_{v,i}$  ( $d_{c,i}$ ) and where  $a_{v,i}$  ( $a_{c,i}$ ) is fraction of variable (check) nodes having degree  $d_{v,i}$  ( $d_{c,i}$ ).  $D_v$  ( $D_c$ ) is the number of different variable (check) node degrees. The LDPC code itself is usually decoded iteratively [47]–[49], and can be viewed as a serially concatenated code with the inner variable node decoder (VND) and the outer check node decoder (CND) [49]. In Fig. 1, an upper VND produces the  $i$ th extrinsic  $L$ -value  $L_{i,E,VND} = L_{A,LDPC} + \sum_{j \neq i} L_{j,A,VND}$  where  $L_{A,LDPC}$  is the deinterleaved version of (3),  $L_{j,A,VND}$  is the  $j$ th *a priori*  $L$ -value going into the variable node (the edge-interleaved version of  $L_{i,E,CND}$ ). A lower VND produces the extrinsic decoder  $L$ -value  $L_{E,LDPC} = \sum_j L_{j,A,VND}$ .

$$L_{E,DET}(c_{j,1}) = \log \frac{p(z_j|c_{j,1} = 1, c_{j,2} = 0, \hat{h}_j) + p(z_j|c_{j,1} = 1, c_{j,2} = 1, \hat{h}_j)e^{L_{A,DET}(c_{j,2})}}{p(z_j|c_{j,1} = 0, c_{j,2} = 0, \hat{h}_j) + p(z_j|c_{j,1} = 0, c_{j,2} = 1, \hat{h}_j)e^{L_{A,DET}(c_{j,2})}}, \quad (3)$$

A CNL produces the  $i$ th extrinsic  $L$ -value  $L_{i,E,CND} = \log \left( \frac{1 - \prod_{j \neq i} \frac{1 - e^{L_{j,A,CND}}}{1 + e^{L_{j,A,CND}}}}{1 + \prod_{j \neq i} \frac{1 - e^{L_{j,A,CND}}}{1 + e^{L_{j,A,CND}}}} \right)$  where  $L_{j,A,CND}$  is the  $j$ th *a priori*  $L$ -value going into the check node (the edge-deinterleaved version of  $L_{i,E,VND}$ ). The extrinsic  $L$ -value at a node of degree  $d_v$  at VND can be calculated with  $d_v$  additions. The  $L$ -value at a node of degree  $d_c$  at CNL can be calculated with  $2d_c$  multiplications, if the  $\tanh$  and  $\tanh^{-1}$  operations are executed by a 2-D lookup table [55]. We refer to [49] for details.

3) *Symbol Mapper*: The tentative decisions are made from the *a posteriori* decoder  $L$ -values via hard decisions and fed back to the “symbol mapper”, which regenerates the OFDM symbols for use by the CFO/channel estimators on the next iteration. The performance improvement using soft instead of hard decisions has been shown to be minimal in [31]–[33], and we have obtained similar results in our receiver simulations.

### C. Structures of Iterative Receivers

We consider three iterative receiver structures in Fig. 1. The same CFOE and CE algorithms are used in all three. At the first iteration, the CFO is estimated based on the CP and the channel is estimated based on pilots as discussed in Section III-A and IV-A. After LDPC decoding, the tentative decisions are made using the *a posteriori* decoder  $L$ -values, and the CFO/channel estimates are further refined as discussed in Section III-B and IV-B.

The Type-1 iterative receiver in Fig. 1a follows the more conventional approach. Multiple inner LDPC decoder iterations  $N_{in}$  are run for every  $N_{out}$  outer estimator/detector  $\leftrightarrow$  LDPC decoder iteration. (The SW is closed only when the inner iterations are completed.) Note that we need to reset the  $L$ -values at  $I_{A,VND}$  once the  $L$ -values at  $I_{E,LDPC}$  are calculated after  $N_{in}$  iterations in order to ensure that  $I_{E,LDPC}$  only depends on  $I_{A,LDPC}$  for the EXIT chart computation [56].

The Type-2 receiver corresponds to Fig. 1b with SW permanently closed. We structure the receiver by combining the estimators, the detector, and the VND as one “super decoder” (left dashed box in the figure) following the proposed architecture in [49]. Messages are thus exchanged between the “super decoder” and the CNL. The Type-2 receiver structure has only one iterative decoding loop and the CFO/channel are updated at every iteration. The Type-3 receiver is identical to Type-2 but SW is closed only at every  $N_{in}$ th iteration. Note that the Type-3 receiver is different from Type-1 in that the LDPC decoder is not re-initialized.

**Remarks :** Both extrinsic probabilities and total *a posteriori* probabilities (APPs) have been considered in the literature for driving the iterative estimator. Only extrinsic information is used for channel estimation in [29], [30]. However, we need to distinguish between feedback to the estimator and to the detector. Since the CFO/channel estimator works in a decision-directed manner, better performance may result by using the total log-APP as proposed in [31]–[34]. Feeding the

total APP to the estimator does not result in direct feedback of the intrinsic information to the decoder.

## III. CFO ESTIMATION

Coarse CFO estimation/correction is performed using preambles as in [57]. The preamble CE is also performed using Least Squares (LS). The number of significant channel taps  $N_c$  corresponds to the  $N_c$  coefficients in  $\hat{\mathbf{f}}_{LS} \in \mathbb{C}^{N_g}$  with largest magnitudes and whose sum power is .99 of the total channel power. The delay spread  $N_f$  is estimated based on the spread of coefficients thus selected.

### A. Initial CFO estimation

Before the CP removal of a data OFDM symbol, initial CFO estimation is performed. There are many CFO estimation algorithms in the literature including [8], [18]. We chose CP-aided CFOE [20]. However, other CFOE algorithms can be utilized as a sub-block of the proposed receivers. Since the CP is a replica of a part of the OFDM symbol, the offset in (1) results in a phase shift of  $2\pi\epsilon$  between the CP and the corresponding part of OFDM symbol. Since the first  $N_f - 1$  samples of the CP are corrupted by ISI, only the ISI free portion of the CP (last  $N_g - N_f + 1$  samples) is used. By using the CFO estimator in [20] and the received samples in (1),

$$\hat{\epsilon} = \frac{1}{2\pi} \angle \left( \sum_{k=N_s-1-N_g+N_f}^{N_s-1} y_{k-N_s}^* y_k \right). \quad (5)$$

If the true CFO  $\epsilon$  is close to  $\pm 0.5$ , there is a possibility the initial CFOE returns  $\hat{\epsilon}$  with the wrong sign due to the  $2\pi$  ambiguity in (5). In order to prevent this effect, if  $|\hat{\epsilon}| > 0.45$  and decoding fails after the iteration process, the iterative process is repeated using initial  $\hat{\epsilon} = -\text{sgn}(\hat{\epsilon})0.5$ .

### B. Iterative CFO estimation

After decoding, hard decisions computed using *a posteriori*  $L$ -values ( $L_{APP,EST}$ ) are fed back to the “symbol mapper” in Fig. 1. Then the estimated symbols  $\{\hat{d}_j\}$  and pilots are multiplexed such that  $\hat{\mathbf{s}} = \mathbf{p} + \hat{\mathbf{d}}$  and converted to the time domain via the IFFT  $\hat{\mathbf{t}} = \mathbf{W}^H \hat{\mathbf{s}}$ . In order to estimate the CFO, the received signal is approximated as

$$\hat{\mathbf{y}} \approx \mathbf{E}(\epsilon) \mathbf{F} \mathbf{W}^H \hat{\mathbf{s}} + \mathbf{n} = \mathbf{E}(\epsilon) \hat{\mathbf{T}} \mathbf{f} + \mathbf{n}, \quad (6)$$

where  $\hat{\mathbf{T}} \in \mathbb{C}^{N_s \times N_f}$  is a truncated circulant matrix with first column given by  $\hat{\mathbf{t}}$ .

To obtain a robust CFO estimation algorithm, we use the unconstrained LS channel estimate  $\hat{\mathbf{f}}_{LS} = (\hat{\mathbf{T}}^H \hat{\mathbf{T}})^{-1} \hat{\mathbf{T}}^H \mathbf{E}(\epsilon) \mathbf{y}$ . Substituting  $\hat{\mathbf{f}}_{LS}$  into the cost function  $\|\mathbf{y} - \mathbf{E}(\epsilon) \hat{\mathbf{T}} \hat{\mathbf{f}}_{LS}\|^2$  yields the CFO estimate,

$$\hat{\epsilon} = \underset{\epsilon}{\text{argmax}} \mathbf{y}^H \mathbf{E}(\epsilon) \hat{\mathbf{T}} (\hat{\mathbf{T}}^H \hat{\mathbf{T}})^{-1} \hat{\mathbf{T}}^H \mathbf{E}(\epsilon) \mathbf{y}. \quad (7)$$

The offset  $\hat{\epsilon}$  can be found through a search in the interval  $[-0.5, 0.5]$ . A similar algorithm is proposed in [8], but only

pilots are utilized therein for CFOE. Since  $\mathbf{T}$  has a circulant structure and  $N_s \gg N_f$ , (7) can be completed in  $O(N_s N_f)$  complex multiplications for each candidate value of  $\epsilon$ .

#### IV. CHANNEL ESTIMATION - MATCHING PURSUITS

##### A. Initial Estimation

The underwater channel is often sparse [44] with many coefficients in  $\mathbf{f} \in \mathbb{C}^{N_f}$  having negligible values. We develop the time domain CE technique for fine channel tracking based on Matching Pursuits in order to exploit this sparsity. The MP algorithm [38]–[43] gives a sub-optimal estimate by detecting the best aligned signal subspace and canceling the effect of the detected subspace iteratively. The MP algorithm for OFDM CE is now derived.

Define  $\mathbf{N} \in \mathbb{Z}^{N_s \times N_s}$  as a diagonal matrix with  $k$ th entry equal to 1 if  $s_k$  is a pilot and 0 otherwise. Define  $\mathbf{r} = \mathbf{G}\tilde{\mathbf{y}}$ , where  $\tilde{\mathbf{y}} = \mathbf{E}(\hat{\epsilon})^H \mathbf{y}$  is the offset-corrected received signal from (2) and  $\mathbf{G} = \mathbf{W}^H \mathbf{N} \mathbf{W}$ . Then assuming zero CFO error,  $\mathbf{r}$  only depends on the pilots  $\mathbf{p}$  as follows.

$$\begin{aligned} \mathbf{r} &\simeq \mathbf{G}(\mathbf{F}\mathbf{W}^H \mathbf{s} + \mathbf{n}) \\ &= \mathbf{W}^H \mathbf{N}(\mathbf{W}\mathbf{F}\mathbf{W}^H)(\mathbf{p} + \mathbf{d}) + \tilde{\mathbf{n}} \\ &= \mathbf{F}\mathbf{W}^H \mathbf{p} + \tilde{\mathbf{n}}. \end{aligned} \quad (8)$$

In (8), we used the fact that the frequency domain channel matrix  $\mathbf{W}\mathbf{F}\mathbf{W}^H = \mathbf{H}$  is diagonal since  $\mathbf{F}$  is a circulant matrix. We first develop the MP algorithm then proceed to discuss the Orthogonal MP version. Define  $\mathbf{a} = \mathbf{W}^H \mathbf{p}$  and rewrite (8) as,

$$\mathbf{r} = \mathbf{A}\mathbf{f} + \tilde{\mathbf{n}}, \quad (9)$$

where  $\mathbf{A} \in \mathbb{C}^{N_s \times N_f}$  is a truncated circulant matrix with first column given by  $\mathbf{a}$ . In order to have a unique solution for  $\mathbf{f}$ ,  $\text{rank}(\mathbf{A}) = N_f$  must be satisfied. It is straight forward to show that at least  $N_f$  pilots are required for  $\text{rank}(\mathbf{A}) = N_f$  [21].

At the first stage of the MP algorithm,  $\mathbf{r}$  is multiplied by  $\mathbf{A}^H$ . Define  $\mathbf{v}_1 = \mathbf{A}^H \mathbf{r}$  and  $\mathbf{B} = \mathbf{A}^H \mathbf{A}$ . We first find the column in the matrix  $\mathbf{A}$  which is best aligned with the signal vector, and this index is denoted  $q_1$ . Then the projection of  $q_1$  is removed from  $\mathbf{v}_1$  and the residual  $\mathbf{v}_2$  is obtained. Now the column in  $\mathbf{A}$ , which is best aligned with  $\mathbf{v}_2$ , is found and a new residual  $q_2$ , is formed. At the  $k$ th iteration,  $q_k$  is given by,

$$q_k = \underset{l}{\text{argmax}} \frac{|(\mathbf{v}_k)_l|^2}{\|(\mathbf{A})_l\|^2}. \quad (10)$$

The channel coefficient estimate at position  $q_k$  is,

$$\hat{f}_{q_k} = \frac{(\mathbf{v}_k)_{q_k}}{\|(\mathbf{A})_{q_k}\|^2}. \quad (11)$$

The new residual vector is then computed as,

$$\mathbf{v}_{k+1} = \mathbf{v}_k - (\mathbf{B})_{q_k} \hat{f}_{q_k}. \quad (12)$$

Steps (10)-(12) are repeated  $N_c$  times with  $N_c \ll N_f$  for a sparse channel.

Since the columns of  $\mathbf{A}$  chosen from (10) are generally not orthogonal, the estimates in (11) may not give the minimal residual error. It is also possible to re-select a previously selected tap, which slows convergence. These problems can

be avoided by using the Orthogonal MP (OMP) algorithm [58]. Define  $\hat{\mathbf{f}}_{omp}^k = [\hat{f}_{q_1}, \hat{f}_{q_2}, \dots, \hat{f}_{q_k}]^T$ . At each iteration after (10), the OMP re-computes the taps according to the least-squares estimate using the subspace chosen by MP,

$$\hat{\mathbf{f}}_{omp}^k = (\mathbf{A}_{omp}^k)^H \mathbf{A}_{omp}^k)^{-1} \mathbf{A}_{omp}^k{}^H \mathbf{r}, \quad (13)$$

where  $\mathbf{A}_{omp}^k \triangleq [\mathbf{A}_{q_1} \mathbf{A}_{q_2} \dots \mathbf{A}_{q_k}]$ . The new residual vector is then computed as,

$$\mathbf{v}_{k+1} = \mathbf{v}_k - (\mathbf{B})_{[q_1, \dots, q_k]} \hat{\mathbf{f}}_{omp}^k. \quad (14)$$

The OMP algorithm requires additional computation due to the matrix inverse. However, we demonstrated that the OMP algorithm outperforms the original MP in [38]. We also refer to [38] where simulation results suggest that time-domain MP is superior to conventional frequency-domain CE using interpolation methods, and thus the additional complexity of MP and OMP is warranted. The convergence properties of MP and OMP algorithm are discussed in [59]. It is readily shown that MP/OMP is locally convergent (although not necessarily to the ML solution), since the error norm  $\|\mathbf{r} - \mathbf{A}\hat{\mathbf{f}}^k\|$  is a non-increasing descent function by design. Furthermore, MP/OMP chooses the index  $q_k$  in (10) on each iteration that leads to the *greatest* decrease in this error norm. It is shown that the MP algorithm outperforms LS estimation in [41] if the channel is sparse as will be further verified using the proposed receiver in Section VI. The OMP algorithm requires  $O(N_s N_c)$  complex multiplies, while  $O(N_s N_f)$  are needed for LSE, thus significant computational saving is achieved if the channel is sparse.

##### B. Iterative Channel Estimation

Based on the iterative CFOE discussed in III-B, the CFO is corrected and (O)MP algorithm is performed based on tentative decisions obtained from the *a posteriori* LDPC decoder  $L$ -value-based hard decisions. We apply the same (O)MP algorithm as described above, but  $\mathbf{N}$  is replaced by the identity matrix  $\mathbf{I}_{N_s}$  in (8), and  $\mathbf{A}$ ,  $\mathbf{B}$  are replaced by  $\hat{\mathbf{T}}$ ,  $\hat{\mathbf{T}}^H \hat{\mathbf{T}}$  respectively in (9)-(14). That is, the tentative decisions are treated as pilots in the iterative CE.

#### V. ITERATIVE RECEIVER DESIGN WITH EXIT CHART

The design of iterative estimators/decoders is of necessity somewhat Ad hoc. However, using the EXIT chart method [49], [60], we are able to evaluate convergence and compare the iterative receiver structures in Fig. 1. All the results in this section are based on the LDPC code introduced in Table I. However, we assume the code block length is infinite, which is common for the EXIT chart analysis. The  $L$ -values corresponding to  $I_{E,DET}$  are assumed to correspond to a binary channel, with output  $y = \pm 1 + v$ , where  $v$  is Gaussian [60], [61]. The distribution of the approximate  $L$ -value  $2y/\sigma_v^2$  is then Gaussian with  $\mu = E[y]$  satisfying  $\mu = \sigma_y^2/2$ . Although the actual detector  $L$ -values are not Gaussian due to the random multipath channel, the Gaussian assumption has nevertheless proven accurate in a wide range of applications, e.g. [49], [56]. We assume the uniform CFO and sparse multipath channel with  $N_c = 8$  as in Section VI.

Note that the LDPC code used here is rather short to facilitate practical implementation. Generally, code lengths of  $10^5$  bits or greater are required so that convergence thresholds from the EXIT chart and actual performance are in good agreement. The EXIT chart analysis for a short code is still valid, but the accuracy is limited [27]. We restrict our discussion to asymptotic performance comparisons.

### A. Type-1 Receiver

The EXIT curve of the ‘‘LDPC decoder’’ in Fig. 1a is obtained via density evolution [56], [61], [62] and plotted in Fig. 2. We choose  $N_{in} = 25$  for practical implementation without losing significant performance. Next, we generate the EXIT curve of the ‘‘estimator/detector’’ in Fig. 1a. The extrinsic information from one component becomes *a priori* information at the other component, thus  $I_{E,LDPC} \rightarrow I_{A,DET}$  and  $I_{E,DET} \rightarrow I_{A,LDPC}$ . The mutual information supplied to the estimator,  $I_{APP,EST}$  is approximated as

$$I_{APP,EST} \approx J \left( \sqrt{[J^{-1}(I_{A,DET})]^2 + [J^{-1}(I_{E,DET})]^2} \right), \quad (15)$$

where  $I_{A,DET}$  and  $I_{E,DET}$  are assumed independent. The function  $J(\sigma_{ch}) = H(X) - H(X|L_{ch}(Y))$  for  $Y = X + N$  where  $X = \pm 1$  with equal probability,  $N$  is zero-mean Gaussian noise with variance  $\sigma_n^2$ , and the channel  $L$ -value  $L_{ch}(Y)$  is again Gaussian with mean  $\pm 2/\sigma_n^2$  and variance  $\sigma_{ch}^2 = 4/\sigma_n^2$ . Efficient numerical approximations to  $J(\sigma_{ch})$  are given in [49]. Since  $I_{E,DET}$  is given as a function of  $I_{A,DET}$ ,  $I_{APP,EST}$  in (15) is actually a function of  $I_{A,DET}$  only. For the EXIT curve of the ‘‘estimator/detector’’ in Fig. 1a, simulations are conducted as follows. For  $0 < I_{A,DET} < 1$ ,  $I_{E,DET}$  is first determined using the EXIT curve with  $N_{in} = 25$  and the corresponding  $I_{APP,EST}$  is calculated by (15). Then  $L_{APP,EST}$  is generated as a Gaussian random variable with variance  $\sigma_{APP}^2 = [J^{-1}(I_{APP,EST})]^2$  and mean  $\sigma_{APP}^2/2$ , followed by the hard decision device. The detector, CFOE and CE are then simulated using the hard decisions, the received vector  $\mathbf{y}$ , and the uniform CFO and Rayleigh channel model in Section VI.

The analysis/simulation approach above yields an EXIT chart. This chart is now used to show that improved power allocation between pilots and symbols can be found. The pilot symbols are equispaced and equipowered as suggested in [53]. In [50]–[52], the power of each pilot subcarrier ( $E_p = |p_k|^2$ ) is boosted over data subcarrier power ( $E_d = |d_k|^2$ ) for rapidly varying channels to ensure estimation quality. However, the power allocation to the pilots can be further reduced for the iterative receiver, such that  $E_p/E_d < 1$  as shown below.

Consider the EXIT chart given in Fig. 2. The total pilot plus data symbol power is fixed, and 0.78 or 0.91 of the total transmit power is allocated to data symbols, which corresponds to  $E_p/E_d = 2$ ,  $E_p/E_d = 1/\sqrt{2}$  respectively. For  $E_p/E_d = 2$  at 1.6 dB of SNR, the EXIT curve of the ‘‘estimator/detector’’ is almost horizontal: The MI with initial estimates ( $I_{E,DET}$  at  $I_{A,DET} = 0$ ) is only slightly less than the MI with perfect symbols ( $I_{E,DET}$  at  $I_{A,DET} = 1$ ). The flatness of the ‘‘estimator/detector’’ curve means that if reliable initial estimates are provided, its MI can converge quickly.

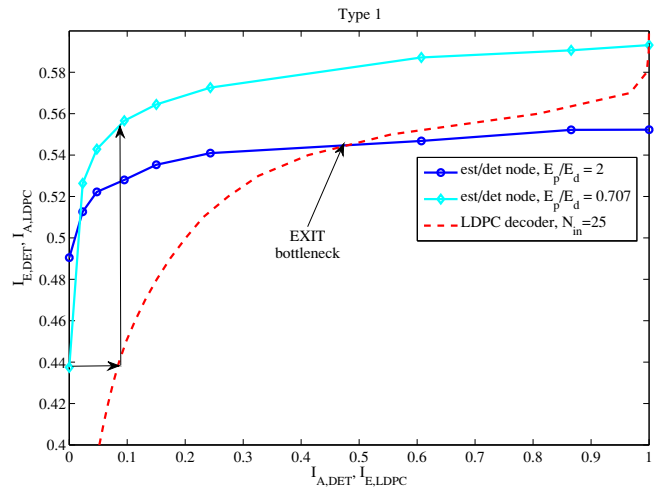


Fig. 2: Type-1 EXIT chart : Pilot power allocation comparison at 1.6 dB of SNR.

However if initial channel information is less accurate, the iterative receiver cannot get over the EXIT bottleneck, even though many iterations are provided. The flatness of the curve limits the enhancement of the iterative process, and the resulting EXIT bottleneck in Fig. 2 suggests a high rate of decoding failure.

The EXIT curve with  $E_p/E_d = 0.707$  is also shown in Fig. 2 at the same SNR. The initial estimates are less reliable than the  $E_p/E_d = 2$  case, since CFOE/CE uses only the lower-power pilot symbols. Therefore worse performance is initially expected for the non-iterative processing. However, we observe that LDPC decoding (see the vertical arrow) provides more reliable information since the power of the data is larger than in the  $E_p/E_d = 2$  scheme. The difference between the MI with initial estimates ( $I_{E,DET}$  at  $I_{A,DET} = 0$ ) and the MI with perfect symbols ( $I_{E,DET}$  at  $I_{A,DET} = 1$ ) is now significant. Even though the initial estimates are less reliable than the  $E_p/E_d = 2$  case, successive iterations yield more reliable information. We observe that the  $E_p/E_d = 0.707$  system is not subject to an EXIT bottleneck. However, note that if  $E_p/E_d$  is too small, then the iterative receiver will also result in decoding failures due to unreliable initial CFO/channel estimates.

In [49], it is shown that the area between the EXIT curves can be interpreted as degradation in MI from capacity, and the capacity approaching optimal code is designed by matching the two curves. We interpret the power allocation technique as another dimension to consider for the optimal design of the iterative estimation process: We are attempting to match the EXIT curves via power allocation. Further power ratio optimization is straightforward by the EXIT chart analysis. However, this is out of scope of the paper, since we are implementing the hardware with short length codes.

### B. Type-2 Receiver

The details of the Type-2 EXIT curve generation are provided in Appendix A. In Fig. 3a, the EXIT chart for the Type-2 receiver with  $E_p/E_d = 2$  is plotted. The ‘‘non-iterative est.’’ plot means that we compute CP and pilot-aided initial estimates and then proceed with LDPC decoding without the

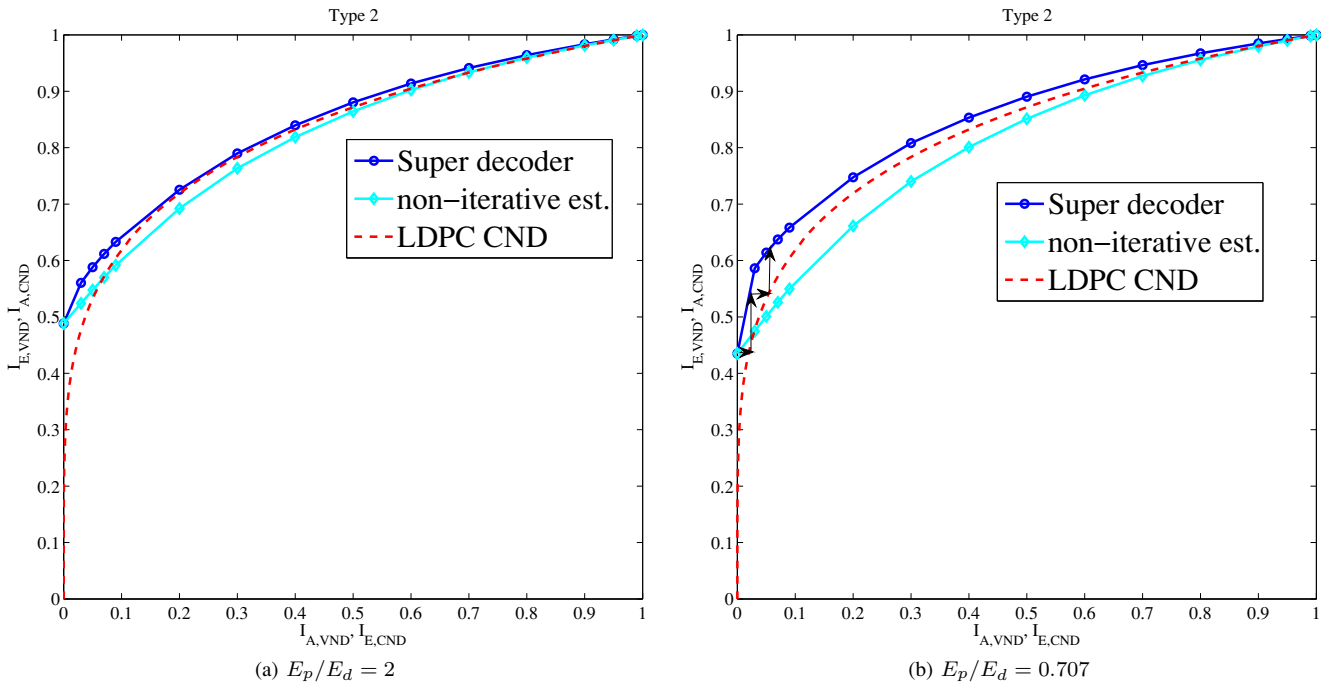


Fig. 3: Type-2 EXIT chart at 1.6 dB of SNR.

subsequent iterative estimation step (SW open). We observe that iterative estimation provides a slightly wider gap, which shows the gain from iterative estimation is negligible in the case of high pilot power. The EXIT chart with  $E_p/E_d = 0.707$  is in Fig. 3b. We see the clear benefits of iterative estimation with the increasing gaps between the two EXIT curves. The non-iterative estimation receiver fails to decode due to the bottleneck while iterative estimation overcomes the EXIT bottleneck. At 1.6 dB of SNR,  $E_p/E_d = 2$  fails to decode, and  $E_p/E_d = 0.707$  succeeds, as similarly seen in the Type-1 receiver.

### C. Convergence Behavior Comparisons

The EXIT chart for both receiver types with  $E_p/E_d = 0.707$  is in Fig. 4. At an SNR of 1 dB, the Type-2 receiver can get through the EXIT bottleneck, while the Type-1 receiver does not converge. This suggests better performance of the Type-2 receiver at low SNRs. The performance in Fig. 4a results from the Type-1 receiver resetting the internal decoder values at every outer iteration. Since the Type-2 receiver in Fig. 4b does not reset the internal decoder  $L$ -values, the MI after the  $n$ th iteration corresponds to  $n$  iterations of LDPC decoding with  $n$  progressively updated estimates, yielding better performance. Note that the Type-2 receiver requires significantly more computation than Type-1, since CFOE/CE is performed at every iteration. (see Table II) On the other hand, the performance improvement for Type-1 in Fig. 4a is limited, even when sufficient computations (iterations) are provided.

### D. Type-3 Receiver

We further reduce the computational complexity from the Type-2 receiver by closing the SW in Fig. 1b only at every  $N_{in}$ th iteration. Since re-estimation is performed after the

LDPC decoding of  $N_{in}$  iterations, more refined tentative decisions are provided to the CFOE/CE compared to the Type-2 receiver. This computationally efficient method also can reduce error propagation due to the unrefined decoder outputs [33], thus the Type-3 is designed in a balanced way such that the estimator and the decoder interact efficiently by passing more refined messages. A similar design was proposed in [33] for Turbo codes, where iterative estimates are computed only if certain criteria are met. The basic difference between Type-1 and Type-3 is that the LDPC decoder does not re-initialize at each iteration. Unfortunately, the EXIT chart analysis of the Type-3 receiver is not feasible since the “super decoder” output varies as the iteration proceeds, thus the Type-3 “super decoder” is a time-varying system. In order to make the EXIT chart analysis tractable, each component should be a time (iteration) invariant system, so that the one-to-one input/output relation of the individual components can be found [60]. The performance of the Type-3 receiver will be provided by BER simulations below instead.

## VI. RESULTS

The system specification for simulations is in Table I. The system is designed so that one OFDM symbol contains one codeword. In simulations, the channel and CFO are generated independently for each OFDM symbol. The channel is generated by random  $N_c = 8$  nonzero tap locations out of  $N_f = 40$  (corresponding to 10 ms in hardware implementation), with each nonzero tap undergoing Rayleigh fading, as similarly modeled in [9], [10]. The CFO is uniformly generated in the range of  $[-0.5, 0.5]$ .

The OMP algorithm is used for the initial/iterative channel estimations. After LDPC encoding, we apply a bit-wise block interleaving ( $\Pi_1$ ) adopted from the IEEE 802.16e standard [50]. We provide the BER of the clairvoyant receiver with perfect CFO/channel knowledge and LDPC decoding with 500

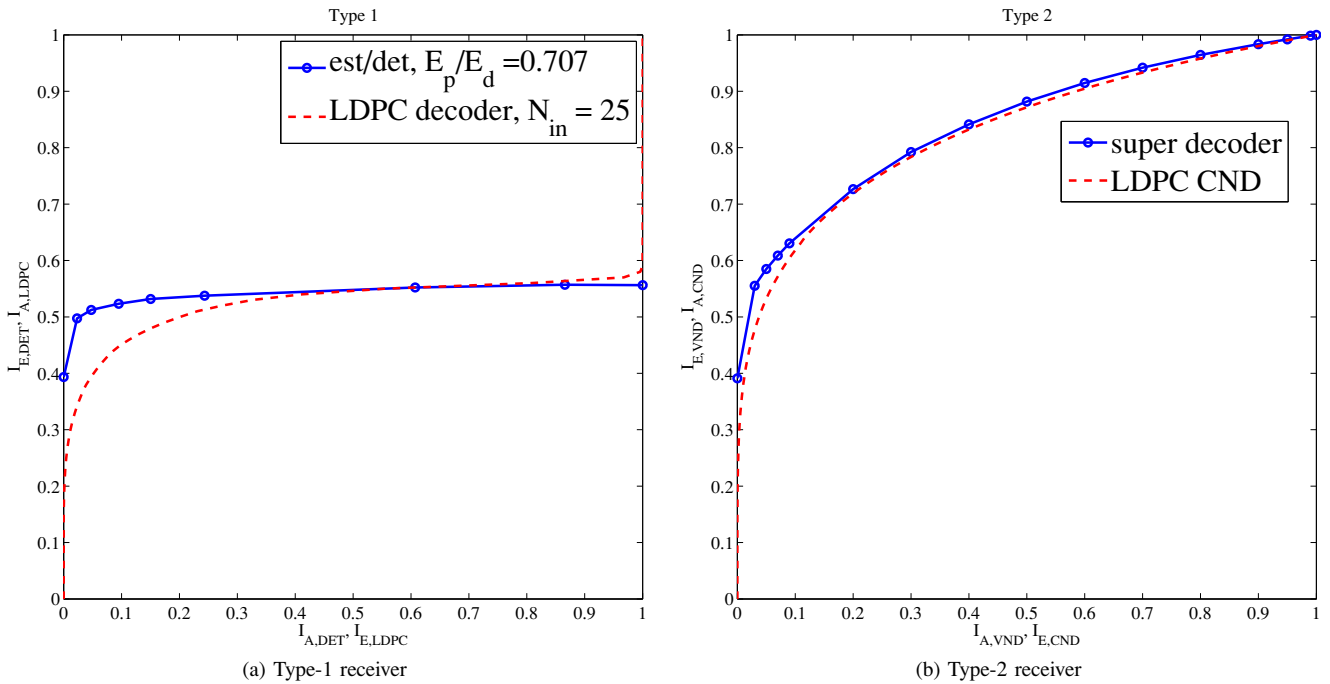


Fig. 4: Performance comparison with EXIT chart at 1 dB with  $E_p/E_d = 0.707$ .

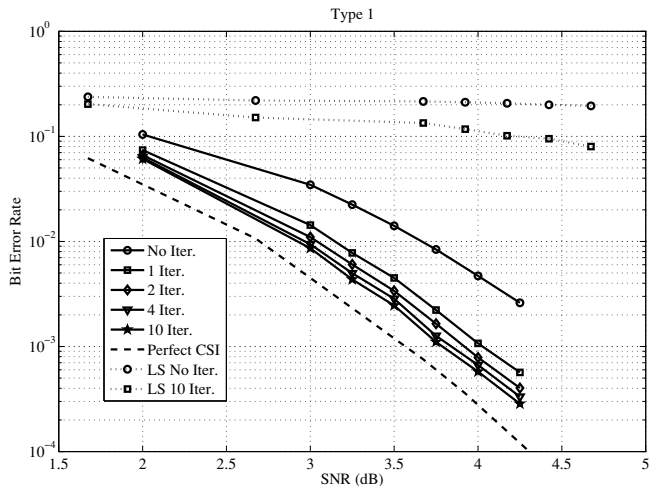


Fig. 5: BERs of Type-1 Receiver with different outer iterations  $N_{out}$  at  $E_p/E_d = 2$ .

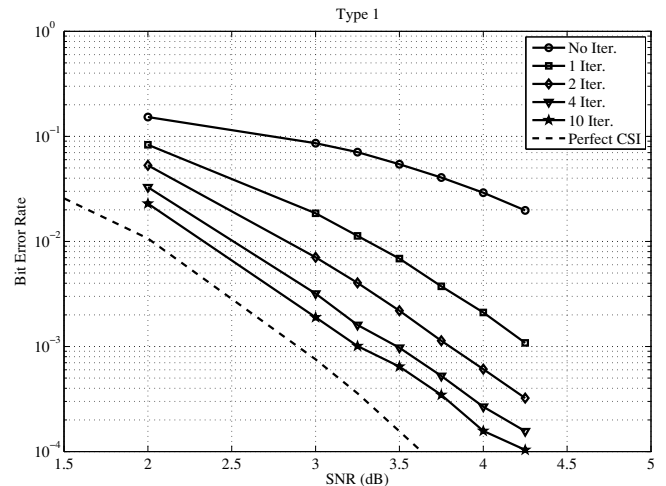


Fig. 6: BERs of Type-1 Receiver with different outer iterations  $N_{out}$  at  $E_p/E_d = 0.707$ .

iterations (“Perfect CSI” plots) as a benchmark. The pilots are sent but not utilized for CFOE/CE in this clairvoyant case. Since the LDPC code here is rather short, the simulation results and the thresholds from the EXIT chart do not match exactly. However, the comparative behavior of the iterative receivers is in good agreement as shown below.

A. Type-1 Receiver

We set  $N_{in} = 25$  for the Type-1 receiver. The BERs of the Type-1 receiver with  $E_p/E_d = 2$  are in Fig. 5. We observe that the iterative process yields progressively lower error rates as  $N_{out}$  increases; however, the gain from successive outer iterations becomes negligible. This implies that the power of the iterative processing has not been fully exploited, as predicted by the EXIT chart analysis. The performance with

time-domain least squares channel estimation (LSE), instead of OMP, is also plotted in Fig. 5. We observe poor performance of LSE compared to OMP, since the former does not exploit the sparsity of the channel. The performance of LSE is limited even for iterative processing due to the poor initial estimates. For  $E_p/E_d = 0.707$  in Fig. 6, we see much larger performance increases between successive  $N_{out}$ , implying that the iterative process is more effective. However, more than 10 outer iterations only slightly improve performance. The performance is further compared in Fig. 7, for the Type-1 receiver for different combinations of inner/outer iterations and pilot power allocation. The BER results for the non-iterative receiver with 500 inner LDPC iterations for each pilot scheme are plotted. Note that  $N_{in} > 500$  does not further decrease BER. We first observe that the iterative processing outperforms non-iterative. Regardless of  $E_p/E_d$ , we observe that iterative processing

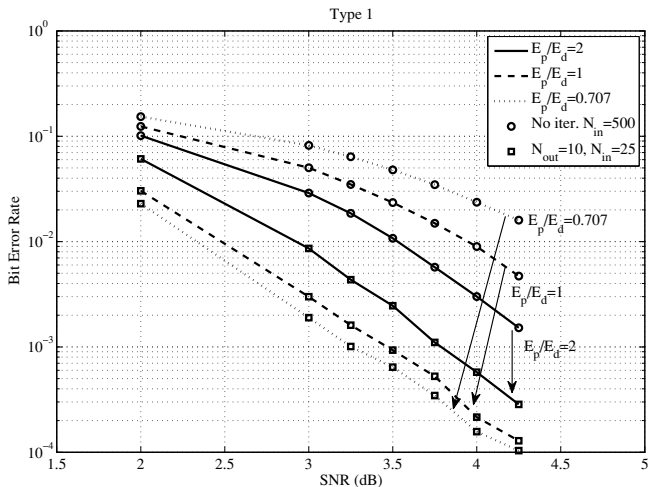


Fig. 7: Performance comparison : Type-1 Receiver.

TABLE II: Computations of each block at each call, for  $(N, K)$  LDPC code.

Blocks	number of flops
CFO estimator	$O(MN_sN_f)$ complex ( $M$ -point CFO search)
Channel estimator	$O(N_sN_c)$ complex
LDPC VND	$N(\sum_i d_{v,i}a_{v,i})(\sum_i d_{v,i}b_{v,i})$ real
LDPC CND	$2K(\sum_i d_{c,i}a_{c,i})(\sum_i d_{c,i}b_{c,i})$ real

significantly improves the performance. Second, we observe  $E_p/E_d = 2$  is better than  $E_p/E_d = 0.707$  for the non-iterative case. This is because the non-iterative receiver only utilizes the pilots for estimation. Third, however,  $E_p/E_d = 0.707$  is better than  $E_p/E_d = 2$  for iterative processing, as we predicted from the EXIT chart analysis. The behavior of  $E_p/E_d = 1$  is between  $E_p/E_d = 2$  and  $E_p/E_d = 0.707$ . The arrows show the performance increase for each pilot allocation scheme. Therefore, the optimal power allocation for the iterative receiver can be quite different from power allocation schemes for the non-iterative receiver. We observe  $E_p/E_d = 0.707, N_{out} = 10$  performs 0.45 dB better than  $E_p/E_d = 2, N_{out} = 10$ , at a BER of  $3 \cdot 10^{-4}$ . In practical implementations, about 11% of the transmitted power can be thus saved with the same performance. Since similar behavior is observed for the other types of receivers, we next report only BER results after reaching the maximum number of iterations.

### B. Performance Comparison

The computational complexity of each block is in Table II for comparative study of the three proposed receivers. The CFOE is the main bottleneck in overall receiver computations. The BERs of all proposed receivers with  $E_p/E_d = 0.707$  are provided in Fig. 8. For all three, the CND node is run 275 times. For the Type-3 receiver, SW is closed at every 25th iteration ( $N_{in} = 25$ ). In these settings, the computational difference between Type-1 and Type-3 is negligible. The Type-3 receiver only needs additional add operations at the upper VND at each outer iteration, which is negligible in terms of overall receiver operation. However, Type-2 needs many more computations, since CFOE/CE is run 275 times for Type-2, in contrast to 11 times for Type-1 and Type-2.

We observe the Type-1 receiver BER in Fig. 8 is slightly worse than the others, while both Type-2 and Type-3 receivers

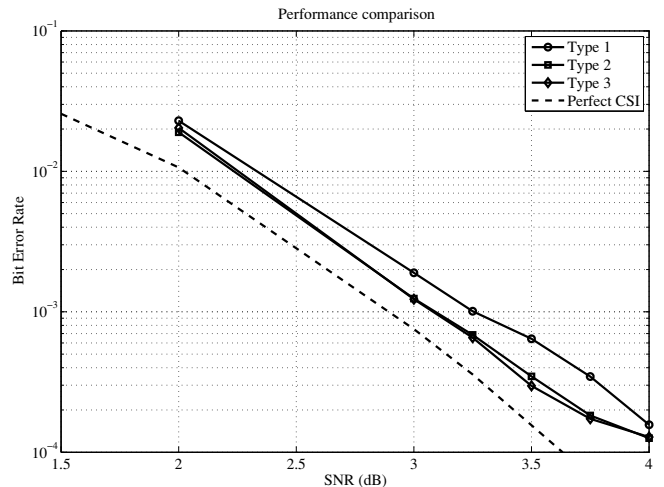
Fig. 8: BERs : Performance Comparison at  $E_p/E_d = 0.707$ .

TABLE III: Underwater Test Results

	$E_p/E_d = 2$	$E_p/E_d = 0.707$
OMP uncoded BER	0.0036	0.0045
spline uncoded BER	0.0055	0.0119
OMP LDPC-coded BER	0	0
spline LDPC-coded BER	0	0

yield almost the same BER. Type-2 and Type-3 perform 0.31 dB better than Type-1 at a BER of  $3 \cdot 10^{-4}$  and about 0.18 dB away from the perfect CSI case. The inferior performance of Type-1 results from the resetting of internal decoder values at every outer iteration. The Type-2 receiver is not preferred due to its computational complexity. The Type-3 receiver offers the best overall performance and the improved performance is obtained at the cost of marginal complexity over Type-1.

### C. Underwater tests

Underwater tests were conducted at Viapahu Lagoon in Moorea, French Polynesia. The OFDM system specification for tests is given in Table I. The transmitter and the receiver were set on the lagoon floor and anchored eliminating physical movement. The depth is about 3m at both locations, the distance is about 330m, and waves and currents were calm. A preamble is included at the start of every packet which contains 25 OFDM data symbols. Timing synchronization is performed by matched filtering to the preamble. The measured delay spread was up to 1.5 ms and 0.5 Hz of maximum Doppler spread was observed. Note that the bottom was mainly coral sand whose lossy nature suppressed multiple surface-bottom interactions.

Since up/down conversion was performed by software, there is minimal CFO due to local oscillator mismatch in the hardware. Indeed, the estimated CFOs are well within  $\hat{\epsilon} < 0.01$ . The measured SNR was about 21.8 dB. The average BER in the field tests are in Table III. A conventional frequency domain CE method based on spline cubic interpolation is also listed as ‘‘spline uncoded’’. First, we observe that OMP CE outperforms the conventional frequency-domain interpolation CE regardless of the pilot power, showing that the OMP algorithm is more suitable in the UAC. Second,  $E_p/E_d = 2$  performs better than  $E_p/E_d = 0.707$  for both CE algorithms. This is reasonable since the estimates are not very accurate with low

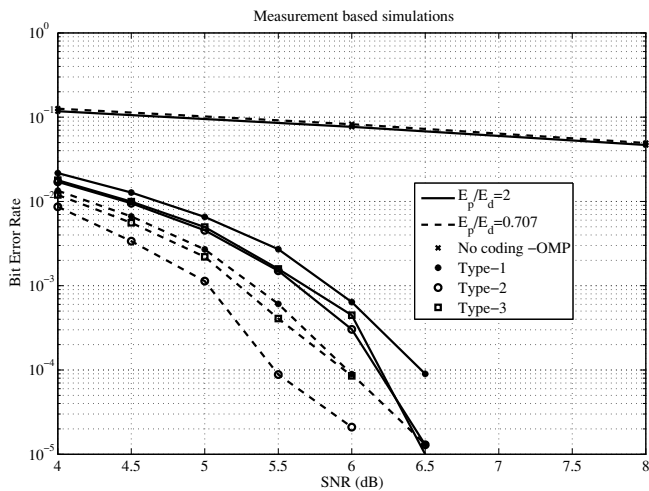


Fig. 9: BERs : Recorded underwater tests with added white noise.

pilot power in non-iterative estimation. Finally, with LDPC decoding, we obtained zero BER for both pilot arrangements. Unfortunately, limitations at the Moorea testbed precluded full testing of iterative processing. Due to the limited distances available, the SNR was sufficiently high that the BER was effectively zero with one LDPC decoding and zero iteration, thus no iterative processing was necessary. Moving platforms with longer distance (or less transmit power) are needed in order to measure the robustness to the time-varying CFO and multipath channel.

In order to better predict the benefits of the iterative receiver in the field, we provide the measurement-based simulation results in Fig. 9 by adding simulated white Gaussian noise to the recorded signal in the underwater tests. First, we observe the BER of the uncoded, non-iterative receiver (No coding-OMP) is not acceptable at low SNR. Fig. 9 clearly indicates the need for LDPC encoding and iterative processing for longer-range UWAC channels where the SNR will be lower. Second, we observe  $E_p/E_b = 0.707$  performs better than  $E_p/E_b = 2$  regardless of the receiver type as predicted by pure simulation results. Note  $E_p/E_b = 2$  is slightly better for the non-iterative case. Finally, the Type-2 and 3 receivers are better than the Type-1 for both pilot allocation schemes. Generally, the behavior of the curves well matches the pure simulation results. However, there is about a 2dB shift of SNR compared to Fig. 8. Also, the Type-2 receiver is slightly better than the Type-3 for  $E_p/E_b = 0.707$ , while Type-2 and 3 showed almost identical performance in pure simulations. The discrepancies between the pure simulation results and noise-augmented field tests may arise due to the non-Gaussian underwater noise. However, definite conclusions about the relative superiority of Type 2 and 3 cannot be inferred due to the testbed limitations.

## VII. CONCLUSIONS

In this paper, iterative LDPC-coded OFDM receivers with CFO and channel estimation are designed for the UAC. A Matching Pursuit channel estimator is developed for the sparse underwater channel. We demonstrated the use of the EXIT chart to optimize the power allocation between pilot and

data for iterative processing. The optimized power allocation strategy for the iterative receiver can be quite different from that of the non-iterative receiver. The asymptotic convergence behavior of different realizations of the iterative receiver was also compared. While all proposed receivers offer excellent performance, the Type-3 receiver is slightly better at the cost of slightly higher complexity than Type-1. Underwater field tests were also conducted. However, testing in more severe underwater environments is required to fully explore the benefits of iterative decoding/estimation.

## ACKNOWLEDGMENT

We would like to thank Tricia Fu, Daniel Doonan, Chris Utley in Prof. Hua Lees group in UCSB and Bridget Benson, Prof. Ryan Kastner in UCSD for the field test and the Moorea LTER for the use of their test facilities.

## APPENDIX A

### TYPE-2 RECEIVER EXIT CHART

1) *LDPC CND*: For the EXIT curve of the “LDPC CND” in Fig. 1b, the output extrinsic information can be approximated as [49],

$$I_{E,CND}(I_{A,CND}, d_c) = 1 - J\left(\sqrt{d_c - 1} \cdot J^{-1}(1 - I_{A,CND})\right), \quad (16)$$

where  $d_c$  is the degree of the check node. Since we use a check-irregular LDPC code, we approximate  $I_{E,CND}$  by averaging over  $b_{c,i}$  such that,

$$I_{E,CND}(I_{A,CND}) \approx \sum_{i=1}^{D_c} b_{c,i} \cdot I_{E,CND}(I_{A,CND}, d_{c,i}). \quad (17)$$

2) *Super Decoder*:  $I_{E,CND}$  becomes  $I_{A,VND}$ , the input of the “super decoder”. For the EXIT curve of the “super decoder” in Fig. 1b, the lower VND of degree  $d_v$  maps  $0 < I_{A,VND} < 1$  into

$$I_{E,LDPC}(I_{A,VND}, d_v) = J\left(\sqrt{d_v} \cdot J^{-1}(I_{A,VND})\right). \quad (18)$$

We average  $I_{E,LDPC}$  in (18) by  $a_{v,i}$  such that,

$$I_{E,LDPC}(I_{A,VND}) = \sum_{i=1}^{D_v} a_{v,i} \cdot I_{E,LDPC}(I_{A,VND}, d_{v,i}), \quad (19)$$

then  $I_{E,LDPC} \rightarrow I_{A,DET}$ . The next step is to obtain  $I_{APP,EST}$ , which requires  $I_{A,DET}$  from (19) and  $I_{E,DET}$  from the previous iteration. However,  $I_{E,DET}$  from the previous iteration (the internal value of the “super decoder”) is not available in the EXIT chart analysis. Thus we approximate the previous  $I_{E,DET}$  based on the LDPC decoder EXIT curve. The appropriate choice of  $N_{in}$  in obtaining  $I_{E,DET}$  is discussed next.

We temporarily denote the previous  $I_{E,DET}$  as  $\tilde{I}_{A,LDPC}$ , and  $I_{A,DET}$  as  $I_{E,LDPC}$  for notational brevity since the terms are functionally equivalent. Then the approximated value of  $\tilde{I}_{A,LDPC}$  can be obtained via  $\tilde{I}_{A,LDPC} = \mathcal{K}^{-1}(I_{E,LDPC}, N_{in} = \infty)$ , where  $I_{E,LDPC} = \mathcal{K}(I_{A,LDPC}, N_{in})$ , and its inverse,  $I_{A,LDPC} = \mathcal{K}^{-1}(I_{E,LDPC}, N_{in})$ . This is the minimum

$$I_{APP,EST}(I_{A,VND}) = J \left( \sqrt{[J^{-1}(I_{E,LDPC}(I_{A,VND}))]^2 + [J^{-1}(\tilde{I}_{A,LDPC})]^2} \right) \quad (20)$$

possible value of the true  $I_{A,LDPC}$ , required to generate a given  $I_{E,LDPC}$  and corresponds to a worst-case simulation of the “super decoder” EXIT curve as further justified below. We plotted the minimum bound of the “super decoder” EXIT curve in Figs. 3 and 4b since the minimum bound is more meaningful for observing convergence behavior. Having approximated  $\tilde{I}_{A,LDPC}$ ,  $I_{APP,EST}$  is obtained by (20).

Next, the new  $I_{E,DET}$  is obtained by simulations using hard decisions generated from  $L$ -values corresponding to (20) and the receiver input  $\mathbf{y}$ , as in the previous Type-1 receiver EXIT chart generation. The MI  $I_{E,DET}$  is thus a function of  $I_{APP,EST}$ , SNR, and  $E_p/E_d$ . The MI  $I_{APP,EST}$  is a function of  $I_{A,VND}$ , yielding  $I_{E,DET}$  as an implicit function,  $I_{E,DET}(I_{A,VND}, \text{SNR}, E_p/E_d)$ . The resulting EXIT curve of the “super decoder” is obtained and given by [49],

$$\begin{aligned} & I_{E,VND}(I_{A,VND}, I_{E,DET}, d_v) \\ &= J \left( \sqrt{(d_v - 1) [J^{-1}(I_{A,VND})]^2 + [J^{-1}(I_{E,DET})]^2} \right). \end{aligned} \quad (21)$$

Finally, we average  $I_{E,VND}$  by  $b_{v,i}$  such that (22) is true. In short, we obtained the EXIT curve of the “super decoder”, in the form

$$I_{E,VND}(I_{A,VND}, \text{SNR}, E_p/E_d). \quad (23)$$

We now go back to the problem of modeling  $\tilde{I}_{A,LDPC}$ . Consider the EXIT curves of the LDPC decoder with different  $N_{in}$ s. In order to generate a given  $I_{E,LDPC}$ , the least required input  $I_{A,LDPC}$  is obtained when the  $N_{in} = \infty$  LDPC decoding is applied. Therefore,  $\tilde{I}_{A,LDPC} = \mathcal{K}^{-1}(\tilde{I}_{E,LDPC}, \infty)$  is the minimum possible value of the true  $I_{A,LDPC}$ , yielding the worst-case  $I_{APP,EST}$  from (20). Furthermore, since the EXIT curves of the “estimator/detector” and upper VND are monotonically increasing functions, the “super decoder” EXIT curve using this worst-case value  $\tilde{I}_{A,LDPC}$  is the minimum bound of the true “super decoder” EXIT curve. With the same reasoning, modeling  $\tilde{I}_{A,LDPC} = \mathcal{K}^{-1}(I_{E,LDPC}, N_{in} = 1)$  yields the maximum bound of the true “super decoder” EXIT curve. However, we observed the bounds are tight in our problem: the MI difference is on the order of  $10^{-3}$ .

## REFERENCES

- [1] D. Kilfoyle and A. Baggeroer, “The state of the art in underwater acoustic telemetry,” *IEEE J. Oceanic Eng.*, vol. 25, no. 1, pp. 4–27, 2000.
- [2] M. Stojanovic, “Recent advances in high-speed underwater acoustic communications,” *IEEE J. Oceanic Eng.*, vol. 21, no. 2, pp. 125–136, 1996.
- [3] A. Bahai and B. Saltzberg, *Multi-carrier digital communications: theory and applications of OFDM*. Springer, 1999.
- [4] T. Pollet, M. V. Bladel, and M. Moeneclaey, “BER sensitivity of OFDM systems to carrier frequency offset and Wiener phase noise,” *IEEE Trans. Commun.*, vol. 43, no. 234, pp. 191–193, 1995.
- [5] A. Salberg and A. Swami, “Doppler and frequency-offset synchronization in wideband OFDM,” *IEEE Trans. Wireless Commun.*, vol. 4, no. 6, pp. 2870–2881, 2005.
- [6] T. Roman, M. Enescu, and V. Koivunen, “Joint time-domain tracking of channel and frequency offset for OFDM systems,” in *IEEE Workshop on Signal Processing Adv. in Wireless Comm.*, 2003, pp. 605–609.
- [7] T. Nyblom, T. Roman, M. Enescu, and V. Koivunen, “Time-varying carrier offset tracking in OFDM systems using particle filtering,” *Proc. IEEE Intern. Symp. on Signal Processing and Information Technology*, pp. 217–220, 2004.
- [8] B. Li, S. Zhou, M. Stojanovic, and L. Freitag, “Pilot-tone based ZP-OFDM demodulation for an underwater acoustic channel,” in *Proc. MTS/IEEE OCEANS*, 2006.
- [9] A. Morozov and J. Preisig, “Underwater acoustic communications with multi-carrier modulation,” in *Proc. MTS/IEEE OCEANS*, 2006.
- [10] W. Lam and R. Ormondroyd, “A coherent COFDM modulation system for a time-varying frequency-selective underwater acoustic channel,” in *Proc. IEEE Intern. Conf. on Electronic Engineering in Oceanography*, 1997, pp. 198–203.
- [11] B. Kim and I. Lu, “Parameter study of OFDM underwater communications system,” in *Proc. MTS/IEEE OCEANS*, vol. 2, 2000, pp. 1251–1255.
- [12] M. Stojanovic, “Low complexity OFDM detector for underwater acoustic channels,” in *Proc. MTS/IEEE OCEANS*, 2006.
- [13] B. Li, M. Stojanovic, L. Freitag, and P. Willett, “Non-uniform Doppler compensation for zero-padded OFDM over fast-varying underwater acoustic channels,” in *Proc. MTS/IEEE OCEANS*, 2007.
- [14] B. Li, S. Zhou, M. Stojanovic, L. Freitag, J. Huang, and P. Willett, “MIMO-OFDM over an underwater acoustic channel,” in *Proc. MTS/IEEE OCEANS*, 2007.
- [15] B. Li, S. Zhou, J. Huang, and P. Willett, “Scalable OFDM design for underwater acoustic communications,” in *Proc. IEEE Intern. Conf. on Acoustics, Speech, and Signal Processing (ICASSP)*, 2008, pp. 5304–5307.
- [16] B. Muquet, Z. Wang, G. Giannakis, M. de Courville, and P. Duhamel, “Cyclic prefixing or zero padding for wireless multicarrier transmissions?” *IEEE Trans. Commun.*, vol. 50, no. 12, pp. 2136–2148, 2002.
- [17] A. Goldsmith, *Wireless communications*. Cambridge University Press, 2005, pp. 387–388.
- [18] X. Ma, C. Tepedelenlioglu, G. Giannakis, and S. Barbarossa, “Non-data-aided carrier offset estimators for OFDM with nullsubcarriers: Identifiability, algorithms, and performance,” *IEEE J. Select. Areas Commun.*, vol. 19, no. 12, pp. 2504–2515, 2001.
- [19] J. Li, G. Liu, and G. B. Giannakis, “Carrier frequency offset estimation for OFDM-based WLANs,” *IEEE Signal Processing Lett.*, vol. 8, no. 3, pp. 80–82, 2001.
- [20] H. Chen and G. Pottie, “A comparison of frequency offset tracking algorithms for OFDM,” in *Proc. IEEE Globecom*, vol. 2, 2003, pp. 1069–1073.
- [21] H. Minn and V. Bhargava, “An investigation into time-domain approach for OFDM channel estimation,” *IEEE Trans. Broadcast.*, vol. 46, no. 4, pp. 240–248, 2000.
- [22] M. Morelli and U. Mengali, “A comparison of pilot-aided channel estimation methods for OFDM systems,” *IEEE Trans. Signal Processing*, vol. 49, no. 12, pp. 3065–3073, 2001.
- [23] X. Ma, H. Kobayashi, and S. Schwartz, “Joint frequency offset and channel estimation for OFDM,” in *Proc. IEEE Globecom*, vol. 1, 2003, pp. 15–19.
- [24] T. Cui and C. Tellambura, “Robust joint frequency offset and channel estimation for OFDM systems,” in *Proc. IEEE Vehicular Technology Conf. (VTC)*, vol. 1, 2004, pp. 603–607.
- [25] H. Minn, V. Bhargava, and K. Letaief, “A combined timing and frequency synchronization and channel estimation for OFDM,” in *Proc. IEEE Intern. Conf. on Communications (ICC)*, vol. 2, 2004, pp. 872–876.
- [26] C. Berrou, A. Glavieux, and P. Thitimajshima, “Near Shannon limit error-correcting coding and decoding: Turbo-codes,” in *Proc. IEEE Intern. Conf. on Communications (ICC)*, vol. 2, 1993, pp. 1064–1070.
- [27] M. Tschler, R. Koetter, and A. Singer, “Turbo equalization: principles and new results,” *IEEE Trans. Commun.*, vol. 50, no. 5, pp. 754–767, 2002.
- [28] M. Valenti and B. Woerner, “Iterative channel estimation and decoding of pilot symbol assisted turbo codes over flat-fading channels,” *IEEE J. Select. Areas Commun.*, vol. 19, no. 9, pp. 1697–1705, 2001.
- [29] F. Sanzi, S. Jelting, and J. Speidel, “A comparative study of iterative channel estimators for mobile OFDM systems,” *IEEE Trans. Wireless Commun.*, vol. 2, no. 5, pp. 849–859, 2003.

$$I_{E,VND}(I_{A,VND}, I_{E,DET}) = \sum_{i=1}^{D_v} b_{v,i} \cdot I_{E,VND}(I_{A,VND}, I_{E,DET}, d_{v,i}). \quad (22)$$

- [30] M. Tuchler, R. Otnes, and A. Schmidbauer, "Performance of soft iterative channel estimation in turbo equalization," in *Proc. IEEE Intern. Conf. on Communications (ICC)*, vol. 3, 2002, pp. 1858–1862.
- [31] H. Niu and J. Ritcey, "Iterative channel estimation and decoding of pilot symbol assisted LDPC coded QAM over flat fading channels," in *Proc. IEEE Asilomar Conf. on Signals, Systems and Computers (ACSSC)*, vol. 2, 2003, pp. 2265–2269.
- [32] M. Oh, H. Kwon, D. Park, and Y. Lee, "Iterative channel estimation and LDPC decoding with encoded pilots," *IEEE Trans. Veh. Technol.*, to appear.
- [33] Y. Huang and J. Ritcey, "Joint iterative channel estimation and decoding for bit-interleaved coded modulation over correlated fading channels," *IEEE Trans. Wireless Commun.*, vol. 4, no. 5, pp. 2549–2558, 2005.
- [34] S. Y. Park, Y. G. Kim, and C. G. Kang, "Iterative receiver for joint detection and channel estimation in OFDM systems under mobile radio channels," *IEEE Trans. Veh. Technol.*, vol. 53, no. 2, pp. 450–460, 2004.
- [35] J. Zheng and B. Rao, "LDPC-coded MIMO systems with unknown block fading channels: soft MIMO detector design, channel estimation, and code optimization," *IEEE Trans. Signal Process.*, vol. 54, no. 4, pp. 1504–1518, 2006.
- [36] H. Niu, M. Shen, J. Ritcey, and H. Liu, "A factor graph approach to iterative channel estimation and LDPC decoding over fading channels," *IEEE Trans. Wireless Commun.*, vol. 4, no. 4, pp. 1345–1350, 2005.
- [37] C. Herzet, N. Noels, V. Lottici, and H. Wymeersch, "Code-aided turbo synchronization," *Proc. IEEE*, vol. 95, no. 6, pp. 1255–1271, 2007.
- [38] T. Kang and R. Iltis, "Matching pursuits channel estimation for an underwater acoustic OFDM modem," in *Proc. IEEE Intern. Conf. on Acoustics, Speech, and Signal Processing (ICASSP)*, 2008, pp. 5296–5299.
- [39] R. Iltis, H. Lee, R. Kastner, D. Doonan, T. Fu, R. Moore, and M. Chin, "An underwater acoustic telemetry modem for eco-sensing," in *Proc. MTS/IEEE OCEANS*, vol. 2, 2005, pp. 1844–1850.
- [40] S. Mallat and Z. Zhang, "Matching pursuits with time-frequency dictionaries," *IEEE Trans. Signal Process.*, vol. 41, no. 12, pp. 3397–3415, 1993.
- [41] S. Cotter and B. Rao, "Sparse channel estimation via matching pursuit with application to equalization," *IEEE Trans. Commun.*, vol. 50, no. 3, pp. 374–377, 2002.
- [42] S. Kim and R. Iltis, "A matching-pursuit/GSIC-based algorithm for DS-CDMA sparse-channel estimation," *IEEE Signal Processing Lett.*, vol. 11, no. 1, pp. 12–15, 2004.
- [43] W. Li and J. Preisig, "Estimation and equalization of rapidly varying sparse acoustic communication channels," *Proc. MTS/IEEE OCEANS*, 2006.
- [44] M. Kocic, D. Brady, and M. Stojanovic, "Sparse equalization for real-time digital underwater acoustic communications," in *Proc. MTS/IEEE OCEANS*, vol. 3, 1995, pp. 1417–1422.
- [45] P. Hoehner, S. Kaiser, P. Robertson *et al.*, "Two-dimensional pilot-symbol-aided channel estimation by Wiener filtering," in *Proc. IEEE Intern. Conf. on Acoustics, Speech, and Signal Processing (ICASSP)*, vol. 3, 1997, pp. 1845–1848.
- [46] C. Wu and D. Lin, "A group matching pursuit algorithm for sparse channel estimation for OFDM transmission," in *Proc. IEEE Intern. Conf. on Acoustics, Speech, and Signal Processing (ICASSP)*, vol. 4, 2006.
- [47] R. Gallager, "Low-density parity-check codes," *IEEE Trans. Inform. Theory*, vol. 8, no. 1, pp. 21–28, 1962.
- [48] D. MacKay, "Good error-correcting codes based on very sparse matrices," *IEEE Trans. Inform. Theory*, vol. 45, no. 2, pp. 399–431, 1999.
- [49] S. ten Brink, G. Kramer, and A. Ashikhmin, "Design of low-density parity-check codes for modulation and detection," *IEEE Trans. Commun.*, vol. 52, no. 4, pp. 670–678, 2004.
- [50] *Part 16: Air interface for fixed and mobile broadband wireless access systems*, IEEE Std. IEEE Std 802.16e-2005, 2005.
- [51] A. Dowler, A. Doufexi, and A. Nix, "Performance evaluation of channel estimation techniques for a mobile fourth generation wide area OFDM system," in *Proc. IEEE Vehicular Technology Conf. (VTC)*, vol. 4, 2002, pp. 2036–2040.
- [52] W. Kirkland and K. Teo, "I/Q distortion correction for OFDM direct conversion receiver," *IEEE Electronics Letters*, vol. 39, no. 1, pp. 131–133, 2003.
- [53] S. Ohno and G. Giannakis, "Capacity maximizing MMSE-optimal pilots for wireless OFDM over frequency-selective block Rayleigh-fading channels," *IEEE Trans. Inform. Theory*, vol. 50, no. 9, pp. 2138–2145, 2004.
- [54] J. Cavers, "An analysis of pilot symbol assisted modulation for Rayleigh fading channels [mobile radio]," *IEEE Trans. Veh. Technol.*, vol. 40, no. 4, pp. 686–693, 1991.
- [55] J. Chen, A. Dholakia, E. Eleftheriou, M. Fossorier, and X. Hu, "Reduced complexity decoding of LDPC codes," *IEEE Trans. Commun.*, vol. 53, no. 8, pp. 1288–1299, 2005.
- [56] J. Hou, P. Siegel, and L. Milstein, "Design of multi-input multi-output systems based on low-density Parity-check codes," *IEEE Trans. Commun.*, vol. 53, no. 4, pp. 601–611, 2005.
- [57] T. Schmidl and D. Cox, "Robust frequency and timing synchronization for OFDM," *IEEE Trans. Commun.*, vol. 45, no. 12, pp. 1613–1621, 1997.
- [58] B. Natarajan, "Sparse approximate solutions to linear systems," *SIAM J. Comput.*, vol. 24, no. 2, pp. 227–234, 1995.
- [59] G. Karabulut and A. Yongacoglu, "Sparse channel estimation using orthogonal matching pursuit algorithm," in *Proc. IEEE Veh. Technol. Conf. (VTC)*, vol. 6, 2004, pp. 3880–3884.
- [60] S. ten Brink, "Convergence behavior of iteratively decoded parallel concatenated codes," *IEEE Trans. Commun.*, vol. 49, no. 10, pp. 1727–1737, 2001.
- [61] S. Chung, T. Richardson, and R. Urbanke, "Analysis of sum-product decoding of low-density parity-check codes using a Gaussian approximation," *IEEE Trans. Inform. Theory*, vol. 47, no. 2, pp. 657–670, 2001.
- [62] T. Richardson, M. Shokrollahi, and R. Urbanke, "Design of capacity-approaching irregular low-density parity-check codes," *IEEE Trans. Inform. Theory*, vol. 47, no. 2, pp. 619–637, 2001.



**Taehyuk Kang** Taehyuk Kang received the B.S. degree in electrical engineering from Yonsei University, Seoul, Korea, in 2001, and the M.S. degree in electrical and computer engineering from the University of California, Santa Barbara (UCSB), in 2006, where he is currently working towards the Ph.D. degree. During 2001–2002, he was a Research Engineer with Optimedia, Inc., where he designed and implemented optical communication systems. In 2006, he was with Samsung Electronics, where he developed 4G MIMO-OFDM relay systems. His

current research focusses on communications theory and signal processing, with an emphasis on MIMO-OFDM for 4G systems, channel estimation, and iterative processing.



**Ronald A. Iltis** Ronald Iltis received the B.A. (Biophysics) from The Johns Hopkins University in 1978, the M.Sc. in Engineering from Brown University in 1980, and the Ph.D. in Electrical Engineering from the University of California, San Diego in 1984. Since 1984, he has been with the University of California, Santa Barbara, where he is currently a Professor in the Department of Electrical and Computer Engineering. His current research interests are in OFDM, software radio, radiolocation, and nonlinear estimation. He has also served as a

consultant to government and private industry in the areas of adaptive arrays, neural networks and spread-spectrum communications.